Effects of Doping Ratio and Thermal Annealing on Structural and Electrical Properties of Boron-Doped ZnO Thin Films by Spray Pyrolysis

2013 Jpn. J. Appl. Phys. 52 065502

(http://iopscience.iop.org/1347-4065/52/6R/065502)

Japanese Journal of Applied Physics **52** (2013) 065502 **REGULAR PAPER**
http://dx.doi.org/**10.7567/JJAP.52.065502**

Effects of Doping Ratio and Thermal Annealing on Structural and Electrical Properties of Boron-Doped ZnO Thin Films by Spray Pyrolysis

Cheng-Chang Yu[1], Yu-Ting Hsu[1], Shao-Yi Lee[2], Wen-How Lan[2]*, Hsin-Hui Kuo[2], Ming-Chang Shih[2], David Jui-Yang Feng[2], and Kai-Feng Huang[1]

[1]*Department of Electrophysics, National Chiao Tung University, Hsinchu 300, Taiwan, Republic of China*
[2]*Department of Electrical Engineering, National University of Kaohsiung, Kaohsiung 811, Taiwan, Republic of China*
E-mail: whlan@nuk.edu.tw

Received August 6, 2012; accepted March 16, 2013; published online May 29, 2013

Boron-doped zinc oxide (BZO) thin films have been fabricated by spray pyrolysis on a glass substrate. The morphology and electrical properties of the thin films were investigated. X-ray diffraction (XRD) and scanning electron microscopy (SEM) analyses were performed. It was found that [B]/[Zn] ratio altered both the microstructure and concentration of the BZO thin films. The film grain size was reduced by increasing the [B]/[Zn] ratio. The highest Hall mobility was 3.65 $cm^2 V^{-1} s^{-1}$ for the undoped ZnO thin film, and the highest carrier concentration of 1.0×10^{19} cm^{-3} was achieved for the as-deposited BZO thin film with [B]/[Zn] = 1.5 at. %. Conductivity was determined at different measurement temperatures and shallow donors provided the dominate conduction mechanism for the as-deposited BZO thin films. After 600 °C annealing, shallow level reduction and donors with a high activation energy of 129 ± 6 meV in the BZO thin films were characterized, and the shallow donors that dominate the carrier concentration for the as-deposited spray-pyrolized BZO thin film were eliminated.

1. Introduction

Transparent conducting zinc oxide (ZnO) thin films have been extensively studied in recent years because of their low resistivity and high optical transmittance in an ultraviolet visible region. ZnO has received much attention because it has numerous applications, such as photovoltaic devices, varistors, and transparent electrodes.[1–3] ZnO is naturally an n-type semiconductor owing to deviation from stoichiometry, and the free charge carriers mainly arise from the shallow donor levels associated with oxygen vacancies and interstitial zinc atoms.[4] Further reduction in the resistivity of zinc oxide can be achieved by doping group III elements, such as B, Al, In, and Ga, in the substitution of zinc atoms to form the donor impurity level.[5–8]

ZnO thin films have been prepared by various techniques. High-quality epitaxial films can be achieved by metal organic chemical vapor deposition methods with different controlled surface morphologies.[9–11] Thus, spray pyrolysis is one of the attractive techniques for obtaining such films,[12,13] because it has advantages of easy fabrication of large-area films without high-vacuum equipment.

The growth of boron-doped zinc oxide (BZO) thin films by RF magnetron sputtering has advantages of better IR transmission than that of aluminum-doped zinc oxide (AZO) thin films,[14] and AZO thin films prepared by successive ion layer adsorption and reaction have deep donor levels.[15] Although BZO thin films deposited by spray pyrolysis have been reported,[16] these BZO thin films showed a large resistivity range[17,18] and there has been no report regarding various resistivities as a function of temperature for the spray-pyrolized BZO thin film. Thus, we have fabricated BZO thin films by spray pyrolysis and analyzed their electrical properties, especially the activation energies of conductivity behaviors.

2. Experimental Procedure

The spray pyrolysis apparatus used in this work consists of a laboratory-built made spraying unit, a substrate holder with a heater, and a ventilator. The distance between the nozzle and the substrate was fixed at 15 cm. One relay was used to control the time circulation with on 2/off 10 s periodically. The flow rate of the solution was controlled at around 1 ml/s. The total deposition time was fixed at 30 min.

An aqueous solution of highly pure zinc acetate [$Zn(CH_3COO)_2 \cdot 2H_2O$] was used as a precursor. The concentration of the solution was 0.2 mol/l. Boron doping was achieved by adding boracic acid (H_3BO_3) to the solution. The atomic ratio between boron and zinc was fixed at 0, 0.25, 0.5, 0.75, and 1 at. %. The films were grown on the glass substrates with thicknesses of around 0.4 μm, and the temperature of the substrate was fixed at 500 °C.

The crystalline structure was obtained by X-ray diffractometry with Cu Kα radiation (Bruker D8). A scanning electron microscopy (SEM) device (Hitachi S-3000H) was used to observe the morphology of the films. The carrier concentration and mobility were obtained by Hall measurement in a four-point probe method (Keithley 2611) at room temperature. Ohmic contacts were achieved by depositing an Al/In metal followed by 350 °C annealing. The van der Pauw method[19] was used to measure the Hall effect and resistivity. Temperature-dependent conductivity measurements were realized by the same four-point probe system with a temperature controlled stage. The annealing procedure was carried out on a conventional furnace with temperature controlled at 600 °C.

3. Results and Discussion

3.1 Characterization of undoped and boron-doped ZnO thin films

SEM micrographs of the undoped and boron-doped ZnO thin films are shown in Fig. 1. It is clearly shown that the surface morphologies of the ZnO thin films were considerably affected by boron doping. The undoped ZnO thin film showed agglomerates that developed from small spiral crystal grains. The granular structures were introduced by boron doping and the grains became smaller with increasing boron content. The films showed pores at doping ratios up to 1 at. %.

The X-ray diffraction (XRD) patterns of the undoped and boron-doped ZnO thin films are shown in Fig. 2. It was found that all the diffraction peaks can be indexed to those of ZnO with a wurtzite structure. The undoped and boron-

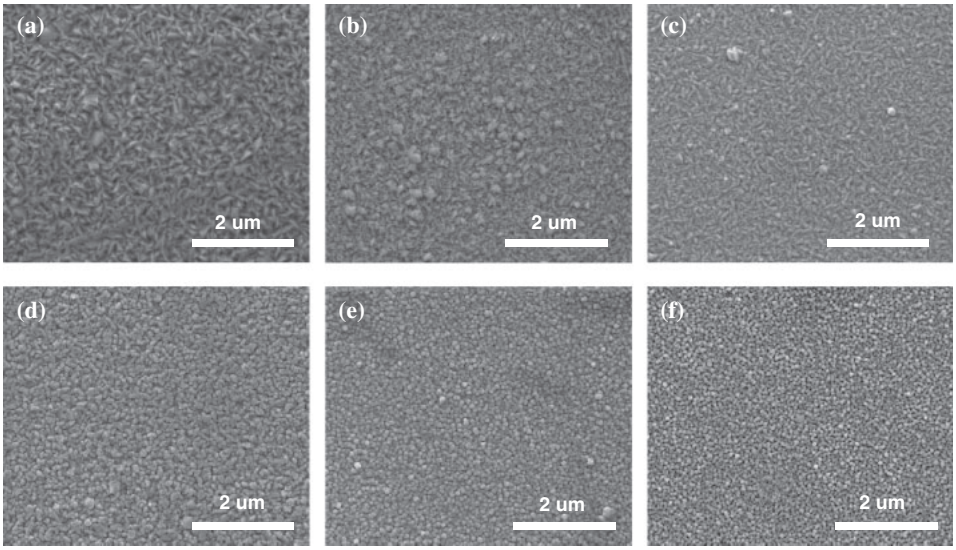

Fig. 1. SEM micrographs of the ZnO thin films with different [B]/[Zn] ratios: (a) undoped ZnO thin film and ZnO thin films doped at (b) 0.25, (c) 0.5, (d) 0.75, (e) 1.0, and (f) 1.5 at. %.

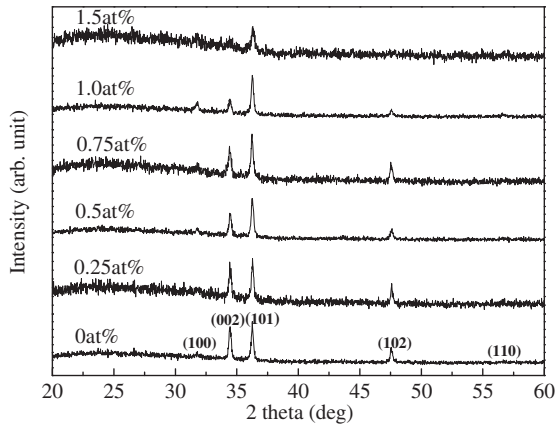

Fig. 2. XRD spectra of the ZnO thin films with different [B]/[Zn] ratios.

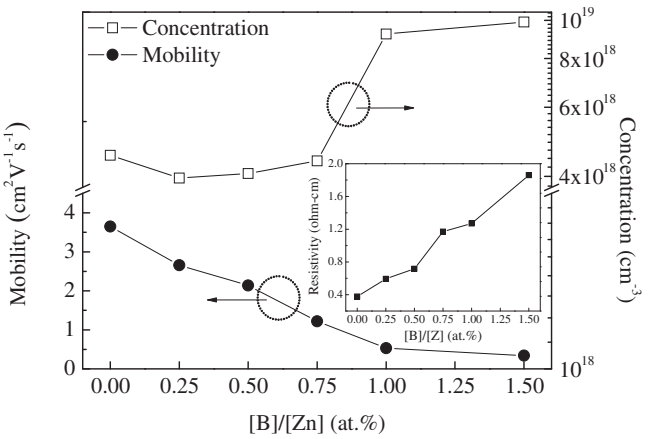

Fig. 3. Carrier concentration and Hall mobility of BZO thin films with different [B]/[Zn] ratios. The inset shows the corresponding resistivity characteristics with different [B]/[Zn] ratios.

doped ZnO films showed two obvious orientations along the (101) and (002) planes. A low (100) intensity was observed in all the samples.[20,21] Furthermore, the (002) and (102) peak intensities decreased with increasing boron content. The film with 1.5 at. % BZO showed a primary (101) peak. Also, the FWHM for this peak was as broad as the increasing boron doping concentration. When boron ions were introduced into the ZnO lattice, the lattice distortion was also introduced,[22] suppressing ZnO grain growth. The worse crystalline quality with highly boron-doped samples can be expected.

3.2 Electrical properties of the undoped and boron-doped ZnO films

All the BZO thin films exhibited n-type conductivity. The carrier concentration and Hall mobility as a function of boron content are shown in Fig. 3. The corresponding resistivity characteristics with different [B]/[Zn] ratios are shown in the inset. As the doping ratio increases from 0 to 1.5 at. %, the carrier concentration increases from around 4.2×10^{18} to $1.0 \times 10^{19}\,\mathrm{cm}^{-3}$. The figure shows that the concentration remains constant with [B]/[Zn] less than 0.75 at. % and increases with [B]/[Zn] greater than 1 at. %. Since there is no significant electron concentration increase with [B]/[Zn] less than 0.75 at. %, the boron atom may be interstitially incorporated into the ZnO structure.[11,23] At higher [B]/[Zn], many boron atoms are introduced and the concentration increases.

The mobility of BZO thin films decreases from 3.4 to $0.34\,\mathrm{cm}^2\,\mathrm{V}^{-1}\,\mathrm{s}^{-1}$ as [B]/[Zn] increases from 0 to 1.5 at. %. With the increase in [B]/[Zn] and the introduction of more boron atoms, the phonon scattering and impurity scattering may play an important role,[24] that is, both may take part in reducing the mobility. As shown in Fig. 1, the grain size decreases as [B]/[Zn] increases. The decrease in grain size allows the grain boundary scattering to increase, also reducing the Hall mobility.[25] The resistivity increases as [B]/[Zn] increases.

To better understand the origin of electrical conduction, film conductivity measurements within the temperature range of 300 to 420 K were carried out. Figure 4 shows the conductivity of the BZO thin films plotted as a function

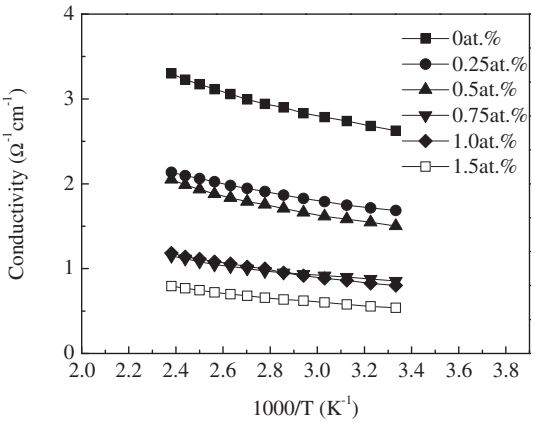

Fig. 4. Conductivity measured at different temperatures for the BZO thin films with different [B]/[Zn] ratios.

Table I. Activation energies (E_A) of the BZO thin films with different [B]/[Zn] values.

[B]/[Zn] (at. %)	Resistivity (Ω cm)	Mobility (cm^2 V^{-1} s^{-1})	Concentration (cm^{-3})	Activation energy E_A (meV)	
				T = 300–360 K Region I	T = 370–420 K Region II
0	0.38	3.65	4.5×10^{18}	20.4	
0.25	0.59	2.66	4.0×10^{18}	21.9	
0.5	0.72	2.14	4.1×10^{18}	23.8	36.3
0.75	1.17	1.22	4.4×10^{18}	20.4	37.5
1.0	1.27	0.53	9.2×10^{18}	35.6	
1.5	1.86	0.34	1.0×10^{19}	34.8	

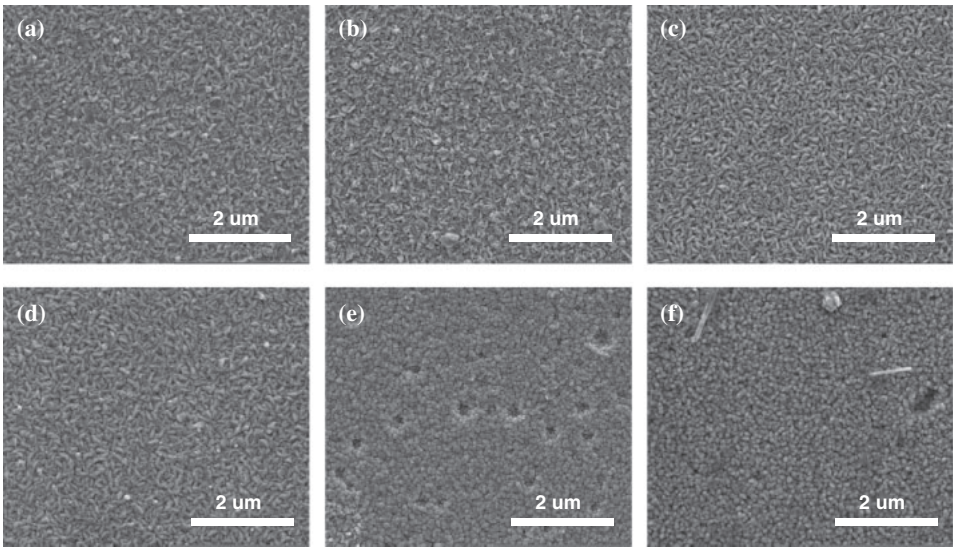

Fig. 5. SEM micrographs of the 600 °C-annealed ZnO thin films with different [B]/[Zn] ratios: (a) undoped ZnO thin film and ZnO thin films doped at (b) 0.25, (c) 0.5, (d) 0.75, (e) 1.0, and (f) 1.5 at. %.

of the inverse measurement temperature. The relationship between conductivity and temperature is given by[26,27)]

$$\sigma = \sigma_0 \exp\left(-\frac{E_A}{kT}\right), \tag{3.1}$$

where σ_0 is the pre-exponential factor, T is the absolute temperature, and k is the Boltzmann constant. The calculated activation energies of the BZO thin films with different [B]/[Zn] values are listed in Table I.

For the as-deposited (0 at. %) ZnO thin film, the activation energy was calculated as 20.5 meV. With 1.5 at. % [B]/[Zn], the activation energy increased to 34.8 meV, implying different conduction behaviors for the boron-doped samples.

It can be seen that as [B]/[Zn] varies from 0.5 to 0.75 at. %, two distinct regions can be observed, suggesting that two different mechanisms contribute to the conduction in the BZO thin films. The two activation behaviors have been observed in many ZnO thin films and two activation energies within different temperature ranges can be achieved.[27–29)] The activation energies corresponding to the two linear slope parts are estimated to be $E_A^I = 22 \pm 2$ meV for region I ($300 \leqq T \leqq 360$ K) and $E_A^{II} = 36 \pm 2$ meV for region II ($370 \leqq T \leqq 420$ K).

For ZnO, the main electrical conduction in these films can be attributed to the contributions of zinc interstitials (Zn_i) and/or oxygen vacancies (V_O) with activation energies of around 30–50 meV[30)] and 0.28–0.32 eV,[31)] respectively. The observed $E_A^{II} = 36 \pm 2$ meV for region II may be assigned to Zn_i, which is a dominant native shallow donor in the as-deposited ZnO thin film.[30)] Since the boron-related activation energy may be around 120–160 meV[32,33)] and cannot be observed in these as-deposited BZO thin films, the shallow donor with $E_A^I = 22 \pm 2$ meV in region I and Zn_i provides the primary conduction mechanism for these as-deposited BZO samples.

To further understand the conduction mechanism, thermal annealing in air atmosphere was carried out. Figure 5 shows the SEM micrographs of these BZO films annealed at 600 °C for 30 min. Compared with that in Fig. 1, a large grain size can be observed in these annealed samples. Annealing is beneficial for the enhancement of Zn–O bonding[29)] and is important for the structure. However, with high [B]/[Zn], for

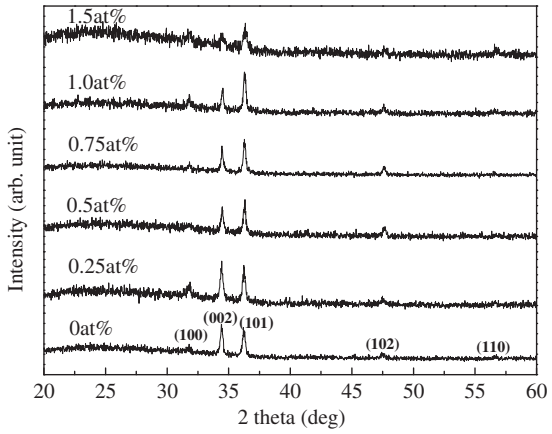

Fig. 6. XRD spectra of the 600 °C-annealed ZnO thin films with different [B]/[Zn] ratios.

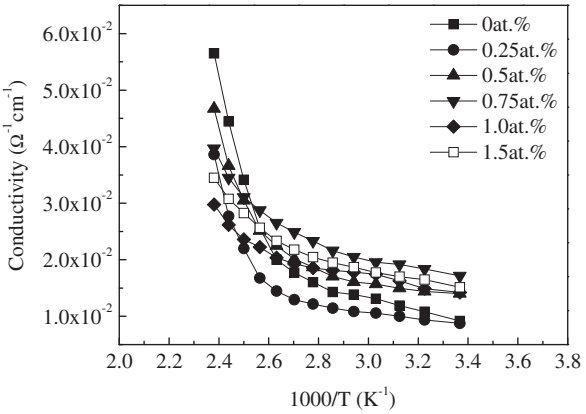

Fig. 7. Conductivity measured at different temperatures for the BZO thin films after 600 °C annealing with different [B]/[Zn] ratios.

Table II. Activation energies (E_A) of the ZnO thin films after 600 °C annealing.

[B]/[Zn] (at. %)	Resistivity (Ω cm)	Mobility ($cm^2 V^{-1} s^{-1}$)	Concentration (cm^{-3})	Activation energy E_A (meV)	
				$T = 300$–360 K Region I	$T = 370$–420 K Region II
0	109	3.75	1.5×10^{16}	43.1	310
0.25	114	2.34	2.4×10^{16}	47.1	292
0.5	71.3	2.14	4.1×10^{16}	46.0	289
0.75	58.3	1.20	8.9×10^{16}	47.5	135
1.0	70.2	0.91	9.8×10^{16}	47.1	127
1.5	66.1	0.81	1.2×10^{17}	45.1	123

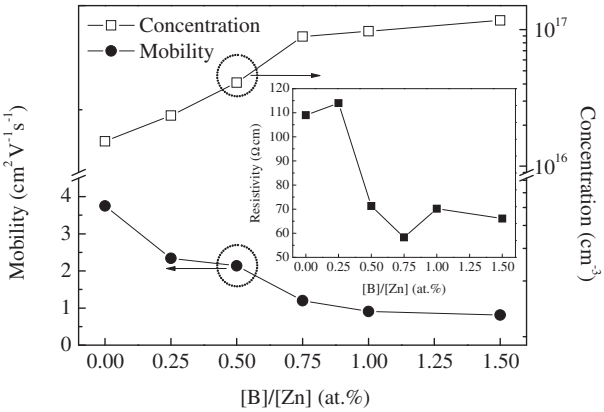

Fig. 8. Carrier concentration and Hall mobility of BZO thin films after 600 °C annealing with different [B]/[Zn] ratios. The inset shows the corresponding resistivity characteristics with different [B]/[Zn] ratios.

example, higher than 1 at. % as shown in Figs. 5(e) and 5(f), some vacancies can be observed.

Figure 6 shows the XRD spectra of the 600 °C-annealed ZnO films with different [B]/[Zn] ratios. Compared with that in Fig. 2, the main peak remains and there is only a small peak FWHM reduction in this figure.

Figure 7 shows the conductivity measured at different temperatures of the ZnO thin films with different [B]/[Zn] ratios after 600 °C annealing. The two distinct regions can be observed in all samples. The extracted activation energies for these regions are shown in Table II. In region I ($300 \leqq T \leqq 360$ K), a low activation energy of around 46 ± 3 meV can be observed. The activation energies of these annealed samples are slightly higher than those of the as-deposited samples. The values are near the reported values of 30–50 meV for Zn_i in the ZnO films,[30] suggesting that the shallow donors of the as-deposited and boron-doped ZnO thin films can be eliminated after 600 °C annealing, and that Zn_i affects the conduction mechanism of these annealed samples. For region II ($370 \leqq T \leqq 420$ K), a larger activation energy can be characterized. For the undoped ZnO thin film, the activation energy is around 310 meV, which implies a neutral oxygen vacancy V_O (0.28–0.32 eV)[31] in the conduction mechanism. As boron content increases, the activation energy decreases. With [B]/[Zn] larger than 0.75 at. %, activation energies of around 135–123 meV can be observed. These activation energies are consistent with the reported boron-associated activation energies of 120–160 meV,[17,32] indicating that the substitution of zinc by born (B_{Zn}) can be observed clearly in the samples with [B]/[Zn] larger than 0.75 at. %.

Compared with the activation energy variation for the as-deposited and annealed samples, it was found that the shallow donors with $E_A^I = 22 \pm 2$ meV can be eliminated after annealing. In the spray pyrolysis method, there may be some hydrogen species incorporated into the as-deposited film.[33] The shallow donors may be assigned to the hydrogen-related states.[34–36] After high-temperature annealing, the elimination of hydrogen can be expected and the electrical conduction may be dominated by Zn_i, V_O, and/or B_{Zn}.

Figure 8 shows the Hall mobility and concentration of the BZO thin films with different [B]/[Zn] ratios after 600 °C air annealing. The inset shows the corresponding resistivity characteristics with different [B]/[Zn] ratios. As the concentration increases and the mobility decreases with increasing [B]/[Zn] in the figure, the resistivity shows a relatively low value of around 56 Ω·cm. Compared with the results in Fig. 3, the mobility shows a small increase. A small crystalline improvement can be expected and is consistent with that in XRD results. However, after 600 °C air annealing, concentration reduction can be observed in the undoped and doped samples. Compared with that in Fig. 3,

two-order-magnitude concentration reduction can be observed. A high concentration reduction can be observed in the removal of hydrogen-related states.[37] In this work, by calculating the activation energy, concentration reduction can be assigned to the elimination of hydrogen-related shallow donors.

4. Conclusions

BZO thin films were prepared by spray pyrolysis, and the effects of boron doping on the structure and surface morphology were studied. The undoped and boron-doped ZnO thin films showed two obvious orientations along the (101) and (002) planes with different surface morphologies. Temperature-dependent conduction measurements were performed to determine the activation energy. Shallow donors provided a major conduction mechanism for the as-deposited undoped and boron-doped ZnO thin films. After 600 °C annealing, a reduction in shallow donor concentration occurred. By calculating the activation energy, the conduction mechanism for zinc interstitials, as well as neutral oxygen vacancies and the substitution of zinc by boron, was observed in the undoped and boron-doped ZnO thin films. Annealing was observed to be an important procedure for the reduction in the concentration of shallow donors incorporated into the ultrasonically spray-pyrolized ZnO thin film.

1) T. K. Gupta: J. Am. Ceram. Soc. **73** (1990) 1817.
2) C. P. Fah and J. Wang: Solid State Ionics **132** (2000) 107.
3) D. Calestani, M. Zha, R. Mosca, A. Zappettini, M. C. Carotta, V. Di Natale, and L. Zanotti: Sens. Actuators B **144** (2010) 472.
4) D. C. Look, J. W. Hemsky, and J. R. Sizelove: Phys. Rev. Lett. **82** (1999) 2552.
5) S. H. Jeong, J. W. Lee, S. B. Lee, and J. H. Boo: Thin Solid Films **435** (2003) 78.
6) B. J. Babu, A. Maldonado, S. Velumani, and R. Asomoza: Mater. Sci. Eng. B **174** (2010) 31.
7) L. Xu and X. Li: J. Cryst. Growth **312** (2010) 851.
8) R. B. H. Tahar: J. Eur. Ceram. Soc. **25** (2005) 3301.
9) C. C. Wu, D. S. Wuu, T. N. Chen, T. E. Yu, P. R. Lin, R. H. Horng, and H. Y. Lai: Jpn. J. Appl. Phys. **47** (2008) 746.
10) C. C. Wu, D. S. Wuu, P. R. Lin, T. N. Chen, and R. H. Horng: Chem. Vapor Deposition **15** (2009) 234.
11) X. L. Chen, B. H. Xu, J. M. Xue, Y. Zhao, C. C. Wei, J. Sun, Y. Wang, X. D. Zhang, and X. H. Geng: Thin Solid Films **515** (2007) 3753.
12) F. D. Paraguay, W. L. Estrada, D. R. N. Acosta, E. Andrade, and M. Miki-Yoshida: Thin Solid Films **350** (1999) 192.
13) M. R. Islam and J. Podder: Cryst. Res. Technol. **44** (2009) 286.
14) J.-S. Hur, J. Kim, S. Jang, J.-B. Song, D. Byun, C.-S. Son, J. H. Yun, and K. H. Yoon: J. Korean Phys. Soc. **53** (2008) 442.
15) S. Mondal, K. P. Kanta, and P. Mitra: J. Phys. Sci. **12** (2008) 221.
16) B. J. Lokhande, P. S. Patil, and M. D. Uplane: Physica B **302–303** (2001) 59.
17) A. E. Rakhshani: J. Phys. D **41** (2008) 015305.
18) R. Bel Hadj Tahar and N. Bel Hadj Tahar: J. Mater. Sci. **40** (2005) 5285.
19) L. J. van der Pauw: Philips Res. Rep. **20** (1958) 220.
20) V. Rakhesh and V. K. Vaidyan: J. Optoelectron. Biomed. Mater. **1** (2009) 281.
21) K. E. Lee, M. Wang, E. J. Kim, and S. H. Hahn: Curr. Appl. Phys. **9** (2009) 683.
22) G. Kim, J. Bang, Y. Kim, S. K. Rout, and S. I. Woo: Appl. Phys. A **97** (2009) 821.
23) B. N. Pawar, S. R. Jadkar, and M. G. Takwale: J. Phys. Chem. Solids **66** (2005) 1779.
24) M. L. Addonizio, A. Antonaia, G. Cantele, and C. Privato: Thin Solid Films **349** (1999) 93.
25) S. Y. Myong and J. Steinhauser: Sol. Energy Mater. Sol. Cells **91** (2007) 1269.
26) P. Mitra and J. Khan: Mater. Chem. Phys. **98** (2006) 279.
27) B. Ergin, E. Ketenci, and F. Atay: Int. J. Hydrogen Energy **34** (2009) 5249.
28) M. Caglar, S. Ilican, Y. Caglar, and F. Yakuphanoglu: J. Alloys Compd. **509** (2011) 3177.
29) H. Kordi Ardakani: Thin Solid Films **287** (1996) 280.
30) Ü. Özgür, Ya. I. Alivov, C. Liu, A. Teke, M. A. Reshchikov, S. Doğan, V. Avrutin, S.-J. Cho, and H. Morkoç: J. Appl. Phys. **98** (2005) 041301.
31) J. C. Simpson and J. F. Cordaro: J. Appl. Phys. **63** (1988) 1781.
32) M. Caglar, S. Ilican, Y. Caglar, and F. Yakuphanoglu: J. Alloys Compd. **509** (2011) 3177.
33) E. V. Lavrov: Physica B **404** (2009) 5075.
34) H. K. Ardakani: Thin Solid Films **287** (1996) 280.
35) S. F. J. Cox, E. A. Davis, S. P. Cottrell, P. J. C. King, J. S. Lord, J. M. Gil, H. V. Alberto, R. C. Vilao, J. P. Duarte, N. A. de Campos, A. Weidinger, R. L. Lichti, and S. J. C. Irvine: Phys. Rev. Lett. **86** (2001) 2601.
36) A. F. Kohan, G. Ceder, D. Morgan, and C. G. Van de Walle: Phys. Rev. B **61** (2000) 15019.
37) Y. M. Strzhemechny, H. L. Mosbacker, D. C. Look, D. C. Reynolds, C. W. Litton, N. Y. Garces, N. C. Giles, L. E. Halliburton, S. Niki, and L. J. Brillson: Appl. Phys. Lett. **84** (2004) 2545.